



# Modeling the photocatalytic degradation of formic acid in a reactor with immobilized catalyst

M. F. J. Dijkstra<sup>a,\*</sup>, H. J. Panneman<sup>a</sup>, J. G. M. Winkelman<sup>a</sup>, J. J. Kelly<sup>b</sup>,  
A. A. C. M. Beenackers<sup>a</sup>

<sup>a</sup>University of Groningen, Department of Chemical Engineering, Nijenborgh 4, 9747 AG, Groningen, The Netherlands

<sup>b</sup>University of Utrecht, Debye Institute, P.O. Box 80000, 3508 TA, Utrecht, The Netherlands

## Abstract

A kinetic model for the photocatalytic degradation of formic acid in an immobilized system is presented, including the dependency of the reaction rate on the concentration of formic acid and oxygen, the catalyst layer thickness and the light flux. In the system some external mass transfer limitation occurs which is included in the modeling with experimentally determined values for the mass transfer coefficient of both formic acid and oxygen. The model describes the measurements well. The degradation rate appears to depend linearly on the light intensity. The adsorption of formic acid and oxygen on the catalyst layer appears to play an important role in the degradation rate.

© 2002 Elsevier Science Ltd. All rights reserved.

*Keywords:* Photocatalysis; Water purification; Kinetics; Immobilized

## 1. Introduction

Heterogeneous photocatalysis has emerged as a novel advanced oxidation technology for chemical treatment of water (Hoffmann, Martin, Choi, & Bahnemann, 1995; Mills & Le Hunte, 1997; Fox & Dulay, 1993). The process uses a semiconductor, usually TiO<sub>2</sub>, as the catalyst which is activated with low-energy UV light to generate charge carriers, electrons and holes, in the semiconductor. The electrons and holes form hydroxyl radicals which are assumed to be the main reactants in the degradation of many pollutants like herbicides, pesticides, aliphatics, aromatics, polymers and dyes (Mills, Davies, & Worsley, 1993). The main advantage of heterogeneous photocatalysis over traditional water treatment methods is that the organic pollutants can be totally degraded to water, carbon dioxide and mineral acids (Ollis, Pelizzetti, & Serpone, 1991).

Titanium dioxide consists of nanometer scale particles which are either suspended or immobilized in the reactor. So far, mostly suspended systems have been used to investigate the degradation of a variety of components (in, e.g. an annular immersion type reactor) (Halmann, 1996). However, a major drawback of suspended systems in practical

applications is the costly separation step necessary after the purification. Therefore, an immobilized system will be the preferred alternative for an efficient reactor scalable to industrial sizes, especially since the efficiency of the immobilized system can be comparable to that of the suspended system (Dijkstra et al., 2001). This study focuses on the photocatalytic degradation of a model component, formic acid, in an immobilized system. Formic acid is used because it is easily degraded and no by-products can be formed during the degradation. Therefore it is ideally suited to investigate the influence of the process parameters.

Kinetic models presented in the literature, especially for immobilized systems, very often do not include the influence of the light flux nor the amount of catalyst on the degradation rate, which causes the models to be reactor dependent (Yue, 1992). To be able to optimize a reactor configuration for a pilot or industrial scale, the influence of these process variables on the degradation rate has to be known. To describe the degradation of formic acid in the immobilized system we developed a simple kinetic model which includes the influences of the light flux, amount of catalyst and the concentration variation of both the model component and the oxidant, oxygen, based on reactions occurring at and near the semiconductor surface. The influence of possible mass transfer limitation, often occurring in immobilized photocatalytic systems (Ollis et al., 1991; Ray & Beenackers, 1997),

\* Corresponding author.

E-mail address: [marga.dijkstra@gkss.de](mailto:marga.dijkstra@gkss.de) (M. F. J. Dijkstra).

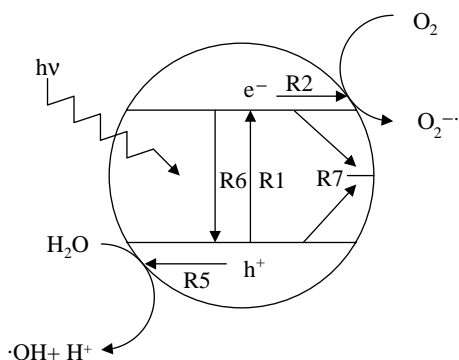


Fig. 1. Simplified reaction scheme of illuminated semiconductor particle. Numbers corresponding to reactions in Table 1.

was taken into account to obtain kinetic parameters independent of the reactor configuration.

## 2. Model

In heterogeneous photocatalysis,  $\text{TiO}_2$  is illuminated with UV-A light, thus generating electrons and holes in the semiconductor which can participate in various reactions (Hoffmann et al., 1995; Turchi & Ollis, 1990; Gerischer, 1995; Pelizzetti & Minero, 1993). A simplified reaction scheme is presented in Fig. 1 and in Table 1.

To prevent the recombination of the charge carriers, the electrons and holes have to be trapped. The electrons can be trapped by molecular oxygen present in the water, thus forming superoxide radicals (R2). Surface defect states can also trap electrons according to Howe and Grätzel (1985) who showed that the conduction band electrons in an oxygen-free aqueous solution are trapped at the particle surface, possibly with the formation of  $\text{Ti}^{3+}$ . Jacobs (1998) has found that the deposition of Pd from an aqueous  $\text{PdCl}_2$  solution on thin polycrystalline  $\text{TiO}_2$  films still occurs in the dark after previous illumination, also indicating the trapping of electrons in the semiconductor (R3). The holes can be trapped by hydroxide ions or water adsorbed at the semiconductor surface forming hydroxyl radicals (R4 and R5). If the electrons and holes are not trapped, they will recombine and the energy will be lost as heat. Recombination can occur either directly (R6) or indirectly via a trap  $T$  (R7) (Gerischer & Heller, 1991; Martin, Herrmann, Choi, & Hoffmann, 1994). In titanium dioxide the recombination will mainly proceed via indirect recombination.

In literature, the hydroxyl radicals are reported to be the main reactants in the degradation of pollutants (Matthews & McEvoy, 1992; Minero, Aliberti, Pelizzetti, Terzian, & Serpone, 1991; Okamoto, Yamamoto, Tanaka, Tanaka, & Itaya, 1985; Turchi & Ollis, 1990), but the photogenerated holes can also attack the pollutants directly (Chen, Zahraa, Bouchy, Thomas, & Bottero, 1995; Dillert & Bahnemann, 1996). The degradation of formic acid is reported to proceed

Table 1

Main reactions occurring during photocatalysis (Hoffmann et al., 1995; Turchi & Ollis, 1990; Gerischer, 1995; Pelizzetti & Minero, 1993; Blake, Webb, Turchi, & Magrini, 1991; Chen, Ollis, Rulkens, & Bruning, 1999; Carraway, Hoffman, & Hoffmann, 1994)

Process	Reaction	Rate
Excitation	$\text{TiO}_2 + h\nu \rightarrow e_{cb}^- + h_{vb}^+$	$ega_{\text{ext}}$ (R1)
Trapping	$e_{cb}^- + \text{O}_{2,\text{ads}} \leftrightarrow \cdot\text{O}_{2,\text{ads}}$	$k_{2+n}[\text{O}_{2,\text{ads}}]a_s$ (R2)
	$e_{cb}^- + T \leftrightarrow T^-$	(R3)
	$h_{vb}^+ + \text{OH}_{\text{ads}}^- \leftrightarrow \cdot\text{OH}_{\text{ads}}$	(R4)
	$h_{vb}^+ + \text{H}_2\text{O}_{\text{ads}} \leftrightarrow \cdot\text{OH}_{\text{ads}} + \text{H}^+$	$k_{5+} \kappa p[\text{H}_2\text{O}_{\text{ads}}]a_s = k_{5+}^1 p a_s$ (R5a) $k_{5-} [\cdot\text{OH}_{\text{ads}}]a_s$ (R5b)
Recombination (direct)	$e_{cb}^- + h_{vb}^+ \rightarrow \text{heat}$	(R6)
	(indirect)	$e_{cb}^- + T \leftrightarrow T^-$
$h_{vb}^+ + T^- \rightarrow T$		$k_{7b} p [T^-] a_s$ (R7b)
Reaction	$\cdot\text{OH}_{\text{ads}} + \text{HCOOH}_{\text{ads}} \rightarrow \text{HCOO} \cdot + \text{H}_2\text{O}$	$k_8 [\cdot\text{OH}_{\text{ads}}] [\text{FA}_{\text{ads}}] a_s$ (R8)
	or	$h_{vb}^+ + \text{HCOOH} \leftrightarrow \text{HCOO} \cdot + \text{H}^+$ (R9) $\text{HCOO} \cdot + \text{O}_2 \rightarrow \text{CO}_2 + \text{H}^+ + \text{O}_2^- \cdot$ (R10)
Radical reactions	$\text{O}_2^- \cdot + \text{H}^+ \rightarrow \text{HO}_2 \cdot$	(R11)
	$\text{HO}_2 \cdot + e^- \rightarrow \text{HO}_2^-$	(R12)
	$\text{HO}_2^- + \text{H}^+ \rightarrow \text{H}_2\text{O}_2$	(R13)
	$2\text{HO}_2 \cdot \rightarrow \text{H}_2\text{O}_2 + \text{O}_2$	(R14)
	$\text{O}_2^- \cdot + \text{HO}_2 \cdot \rightarrow \text{O}_2 + \text{HO}_2^-$	(R15)
	$\text{H}_2\text{O}_2 + e^- \rightarrow \cdot\text{OH} + \text{OH}^-$	(R16)
	$\text{H}_2\text{O}_2 + \cdot\text{OH} \rightarrow \text{H}_2\text{O} + \text{HO}_2 \cdot$	(R17)
	$2 \cdot\text{OH} \rightarrow \text{H}_2\text{O}_2$	(R18)
Adsorption	$\text{site}_{\text{O}_2} + \text{O}_2 \leftrightarrow \text{O}_{2,\text{ads}}$	(R19)
	$\text{site}_{\text{FA}} + \text{HCOOH} \leftrightarrow \text{HCOOH}_{\text{ads}}$	(R20)

both via indirect (the hydroxyl route) (Kesselman, Weres, Lewis, & Hoffmann, 1997; Peterson, Turner, & Nozik, 1991) and via direct attack (uptake of  $h^+$ ) (Bideau, Claudel, & Otterbein, 1980; Pelizzetti & Minero, 1993; Prairie, Evans, Stange, & Martinez, 1993; Upadhy & Ollis, 1997), presented in Table 1 as reaction (R8) and (R9), respectively. Following the measurements of Kesselman et al. (1997), the indirect route is taken as the dominant reaction route.

To obtain a simple model which describes the macroscopic phenomena in the reactor with a reasonable amount of fitting parameters, several assumptions have been made. According to Kelly and Vanmaekelbergh (1998) the recombination and trapping of the electrons and holes occurs at the surface of nanoporous layers of semiconductors and bulk recombination is negligible. The generation of electrons and holes by the reverse of reactions (R2) and (R5) is negligible compared to the production via reaction R1. Furthermore, it is assumed that the semiconductor layer is totally accessible for both the pollutant and oxygen, and water without any diffusion limitation in the pores.

Hydroxyl radicals are formed both by holes via reaction R5 and by electrons via the superoxide radical,  $O_2^-$ , which via various radical reactions (R11)–(R15) can lead to the formation of a hydroxyl radical from hydrogen peroxide (R16). The latter production of hydroxyl radicals will be proportional to the direct formation via (R5) and can therefore be taken into account in the total production of hydroxyl radicals by adding a factor  $\kappa$  to the reaction rate of (R5) as is also done by Turchi and Ollis (1990).

The reaction rate is related to the total generation rate,  $g$ , of electrons and holes in the layer. The reactions occurring at the catalyst surface are related to the concentration of reactants in the reactor. The generation rate of electron-hole pairs by a photon with an energy equal to or larger than the band gap energy ( $h\nu \geq E_{\text{gap}}$ ) is given by Butler (1977):

$$g(x, \lambda) = I_0(\lambda)\alpha(\lambda) \exp(-\alpha(\lambda)x), \quad (1)$$

where  $I_0(\lambda)$  is the photon flux for a certain wavelength (Einstein  $\text{m}^{-2} \text{s}^{-1} \text{nm}^{-1}$ ),  $\alpha$  is the optical absorption coefficient of the semiconductor layer ( $\text{m}^{-1}$ ),  $x$  is the distance into the semiconductor (m) and  $\lambda$  is the wavelength of the light (nm). The optical absorption coefficient is determined experimentally as a function of the wavelength for a dip-coated layer of titanium dioxide. The value of the optical depth obtained, which is the reciprocal of  $\alpha$  (Tan et al., 1994), was found to be 0.3  $\mu\text{m}$  for  $\lambda$  is 350 nm. This value is equal to the value of the optical depth found by Jongh and Vanmaekelbergh (1996) for a dipcoated layer of Degussa P25  $\text{TiO}_2$ .

The total wavelength specific generation rate of electrons and holes is found from Eq. (1) by integration over the thickness of the semiconductor layer:

$$g(\lambda) = I_0(\lambda) - I_0(\lambda) \exp(-\alpha(\lambda)d_L), \quad (2)$$

where  $d_L$  is the thickness of the semiconductor layer (m). Because  $\alpha$  and the light flux are a function of the wavelength of the light,  $g(\lambda)$  should be integrated over the spectrum of the lamp to obtain the total generation rate of electrons and holes:

$$g = \int_{\lambda_1}^{\lambda_2} g(\lambda) d\lambda, \quad (3)$$

where the integration is over the relevant part of the lamp spectrum ( $\lambda \leq 387 \text{ nm}$ ). This formula is used to obtain the values of  $g$  as a function of the light flux and the layer thickness in the kinetic model (reaction R1).

Four different reaction schemes are often described to occur in photocatalysis: (I) reaction between an adsorbed hydroxyl radical and an adsorbed organic pollutant, (II) reaction between both molecules free in solution, (III) reaction between a free pollutant and an adsorbed hydroxyl radical, and (IV) reaction between an adsorbed pollutant and a free hydroxyl radical (Turchi & Ollis, 1990). Of these different schemes mostly one option is taken dominant in the degradation. If so, other routes have not to be taken into account in the kinetic analysis (Turchi & Ollis, 1990; Emeline, Ryabchuk, & Serpone, 2000). Since desorption of hydroxyl radicals into the solution is unlikely (Lawless, Serpone, & Meisel, 1991), the reactions including free hydroxyl radicals are not considered. The rate of disappearance of the model component can be represented by the reaction between an adsorbed hydroxyl radical and adsorbed formic acid (Turchi & Ollis, 1990; Emeline, Ryabchuk, & Serpone, 2000) (R8):

$$R_{FA} = k_8[\cdot\text{OH}_{\text{ads}}][FA_{\text{ads}}]a_s. \quad (4)$$

In the discussion below, also the reaction of adsorbed formic acid and a hole (R9) is discussed and compared with relation 4. A further option, reaction between free formic acid and adsorbed hydroxyl radicals is also discussed.

The steady-state approximation for the total concentration of electrons, holes, trapped electrons ( $T^-$ ) and hydroxyl radicals is used:

$$\frac{dn}{dt} \approx 0 = ega_{\text{ext}} - k_{7a}n[T]a_s - k_{2+n}[O_{2,\text{ads}}]a_s, \quad (5)$$

$$\frac{dp}{dt} \approx 0 = ega_{\text{ext}} - k_{7b}p[T^-]a_s - k_{5+}^1pa_s, \quad (6)$$

$$\frac{d[T^-]}{dt} \approx 0 = k_{7a}n[T]a_s - k_{7b}p[T^-]a_s, \quad (7)$$

$$\begin{aligned} \frac{d[\cdot\text{OH}_{\text{ads}}]}{dt} \approx 0 = & k_{5+}^1pa_s - k_{5-}[\cdot\text{OH}_{\text{ads}}]a_s \\ & - k_8[\cdot\text{OH}_{\text{ads}}][FA]a_s, \end{aligned} \quad (8)$$

in which  $n$  is the concentration of electrons ( $\text{mol m}_{\text{react}}^{-3}$ ),  $a_{\text{ext}}$  is the specific external surface area ( $\text{m}_{\text{ext}}^2 \text{m}_{\text{react}}^{-3}$ ),  $a_s$  is the specific internal surface area ( $\text{m}_{\text{int}}^2 \text{m}_{\text{react}}^{-3}$ ),  $[T]$  is the concentration traps in the layer ( $\text{mol m}_{\text{react}}^{-3}$ ),  $p$  is the concentration

of holes ( $\text{mol m}_{\text{reac}}^{-3}$ ) and  $e$  is the equivalence constant correlating the moles of charge carriers produced to the Einsteins of photons absorbed by the catalyst, equal to  $1 \text{ mol Einst}^{-1}$ . The concentration of the adsorbed oxygen and formic acid per unit reactor volume can be calculated with the adsorption equilibria assuming non-competitive adsorption (Turchi & Ollis, 1990):

$$[\text{O}_{2,\text{ads}}] = K_{19}[\text{O}_2][\text{site}_{\text{O}_2}], \quad (9)$$

$$[\text{FA}_{\text{ads}}] = K_{20}[\text{FA}][\text{site}_{\text{FA}}], \quad (10)$$

where the concentration of vacant sites is related to the total concentration of sites:

$$[\text{site}_{\text{O}_2}] = [\text{site}_{\text{O}_2,\text{tot}}] - [\text{O}_{2,\text{ads}}], \quad (11)$$

$$[\text{site}_{\text{FA}}] = [\text{site}_{\text{FA},\text{tot}}] - [\text{FA}_{\text{ads}}]. \quad (12)$$

The concentration of adsorbed hydroxyl radicals can be determined from Eqs. (5) to (12) and the reaction rate (Eq. (4)) can be written as

$$R_{\text{FA}} = \frac{ek_8gk_2+K_{19}[\text{site}_{\text{O}_2,\text{tot}}][\text{O}_2]K_{20}[\text{site}_{\text{FA},\text{tot}}][\text{FA}]a_{\text{ext}}}{((k_2+K_{19}[\text{site}_{\text{O}_2,\text{tot}}] + k_{7a}K_{19}[T])[\text{O}_2] + k_{7a}[T])(k_5-K_{20} + k_8K_{20}[\text{site}_{\text{FA},\text{tot}}][\text{FA}] + k_{5-})}. \quad (13)$$

For a constant porosity over the layer, the number of sites will increase linearly with the amount of catalyst:

$$[\text{site}_{A,\text{tot}}] = k_{s,A}w_{\text{cat}}, \quad (14)$$

in which  $k_{s,A}$  is a proportionality constant for component  $A$  and  $w_{\text{cat}}$  is the amount of catalyst per square meter ( $\text{g m}^{-2}$ ). This relation is also used for the concentration traps in the layer;

$$[T] = k_Tw_{\text{cat}}. \quad (15)$$

According to Hoffmann et al. (1995) the reaction between electrons and oxygen (R2) is much slower than the trapping of the electrons in the semiconductor (R7a), while also the equilibrium of reaction R5 is at the right-hand side, implying that  $k_{5-}$  is much smaller than  $k_8$ . With these estimations we can assume that  $k_{2+}[\text{site}_{\text{O}_2,\text{tot}}] \ll k_{7a}[T]$  and  $k_8[\text{site}_{\text{FA},\text{tot}}] \gg k_{5-}$ , respectively. These lead to the simplified kinetic relation

$$R_{\text{FA}} = \frac{k_r eg K_1 w_{\text{cat}} [\text{FA}] K_2 [\text{O}_2] a_{\text{ext}}}{(1 + K_1 w_{\text{cat}} [\text{FA}])(1 + K_2 [\text{O}_2])}, \quad (16)$$

in which

$$k_r = \frac{k_2 + k_{s,\text{O}_2}}{k_{7a} k_T}, \quad (17)$$

$$K_1 = \frac{k_8 K_{20} k_{s,\text{FA}}}{k_{5-}}, \quad (18)$$

$$K_2 = K_{19}. \quad (19)$$

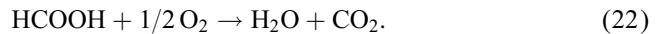
## 2.1. External mass transfer limitation

Systems with immobilized catalysts may suffer from external mass transfer limitation. Then the surface concentrations of formic acid and oxygen differ from the bulk concentrations and can be calculated by considering the mass balance over the film according to the stagnant film model:

$$k_{L,\text{FA}} a_{\text{ext}} (C_{b,\text{FA}} - C_{s,\text{FA}}) = R_{\text{FA}}, \quad (20)$$

$$k_{L,\text{O}_2} a_{\text{ext}} (C_{b,\text{O}_2} - C_{s,\text{O}_2}) = 0.5 R_{\text{FA}}, \quad (21)$$

in which  $k_{L,A}$  is the mass transfer coefficient of component  $A$  ( $\text{m s}^{-1}$ ),  $C_{b,A}$  and  $C_{s,A}$  the bulk and surface concentration of component  $A$ , respectively ( $\text{mol m}^{-3}$ ). The factor 0.5 in Eq. (21) is the stoichiometric constant of oxygen in the overall degradation reaction



The mass balance of a recirculating batch system with relation 16 in terms of surface concentrations is

$$\frac{dC_{b,\text{FA}}}{dt} = - \frac{k_r eg w_{\text{cat}} K_1 C_{s,\text{FA}} K_2 C_{s,\text{O}_2} a_{\text{ext}}}{(1 + w_{\text{cat}} K_1 C_{s,\text{FA}})(1 + K_2 C_{s,\text{O}_2})} \frac{V_{\text{reac}}}{V_{\text{liq}}}, \quad (23)$$

in which  $V_{\text{liq}}$  is the total liquid volume in the recirculating batch system ( $\text{m}^3$ ) and  $V_{\text{reac}}$  is the reactor volume (annular space,  $\text{m}^3$ ). The system of Eqs. (2), (3), (20), (21), (23) was fitted to experimental degradation data to obtain the values of the parameters  $k_r$ ,  $K_1$  and  $K_2$ .

## 2.2. Internal diffusion limitation

In relation (23) the influence of possible internal diffusion limitation of formic acid and oxygen on the reaction rate has been neglected. The layer was assumed to be totally accessible for the reacting components. This assumption can be verified by calculating the effectiveness factor, which is equal to (Froment & Bischoff, 1979)

$$\eta = \frac{\text{rate of reaction with pore diffusion resistance}}{\text{rate of reaction at surface conditions}} \quad (24)$$

with no and complete diffusion limitation for  $\eta = 1$  and 0, respectively. According to Westerterp, Van Swaaij, and Beenackers (1984) the effectiveness factor can be calculated with

$$\eta = \frac{\tanh \phi}{\phi}, \quad (25)$$

in which  $\phi$  is the Thiele modulus (–), whose definition depends on the reaction kinetics. To be able to use an explicit relation in our system two simplified limiting situations can be identified assuming constant activity over the layer (actually the light intensity and thus the activity varies over the layer thickness):

1. The formic acid concentration is relatively low ( $C_{s,FA}/C_{s,O_2} < 0.4$ ). Then, the possible diffusion limitation will occur for formic acid only. The kinetic model can be simplified to a Langmuir–Hinshelwood type of kinetic model dependent on the formic acid concentration:

$$-R_{FA,cat} = \frac{k_{FA}C_{s,FA}}{1 + w_{cat}K_1C_{s,FA}}$$

$$\text{with } k_{FA} = \frac{k_r eg K_1 K_2 w_{cat} C_{s,O_2} A_{ext}}{1 + K_2 C_{s,O_2} V_{cat}}, \quad (26)$$

in which  $R_{FA,cat}$  is the reaction rate of formic acid per unit catalyst volume ( $\text{mol m}^{-3} \text{s}^{-1}$ ),  $A_{ext}$  is the external catalyst area ( $\text{m}^2$ ) and  $V_{cat}$  is the catalyst volume ( $\text{m}^3$ ).

2. If the formic acid concentration is relatively high ( $C_{s,O_2}/C_{s,FA} < 0.1$ ), oxygen diffusion is assumed to be limiting. Then, the kinetic model can be simplified to

$$-R_{FA,cat} = \frac{k_{O_2}C_{s,O_2}}{1 + K_2C_{s,O_2}}$$

$$\text{with } k_{O_2} = \frac{k_r eg K_1 K_2 w_{cat} C_{s,FA} A_{ext}}{1 + w_{cat}K_1C_{s,FA} V_{cat}}. \quad (27)$$

For these types of Langmuir–Hinshelwood kinetics, the Thiele modulus is defined as (Westertep et al., 1984)

$$\phi = \frac{d_L \sqrt{(k_{LH}/2K_{ads}D_{eff,A})(K_{ads}C_{s,A})/(1 + K_{ads}C_{s,A})}}{\sqrt{C_{s,A} - (1/K_{ads})\ln(1 + K_{ads}C_{s,A})}}$$

$$\text{for } -R = \frac{k_{LH}C_{s,A}}{1 + K_{ads}C_{s,A}}, \quad (28)$$

in which  $k_{LH}$  is the Langmuir–Hinshelwood reaction rate constant and  $K_{ads}$  is the Langmuir–Hinshelwood adsorption constant.  $D_{eff,A}$  is the effective diffusivity of component  $A$  which follows from

$$D_{eff,A} = \frac{\varepsilon_{cat}}{\tau} D_A, \quad (29)$$

with  $\varepsilon_{cat}$  the porosity of the catalyst,  $\tau$  the tortuosity and  $D_A$  the diffusion coefficient of component  $A$ . For the tortuosity factor the value of  $\sqrt{3}$  is typical for loose random structures (Froment & Bischoff, 1979). The porosity of the catalyst was determined experimentally as 0.6 by means of SEM photography. The values of the effectiveness factors now can be determined for the situation where either the oxygen or the formic acid concentration is lowest and thus its diffusion limitation, if any, is dominating. Relatively low oxygen concentrations exist at the beginning of the

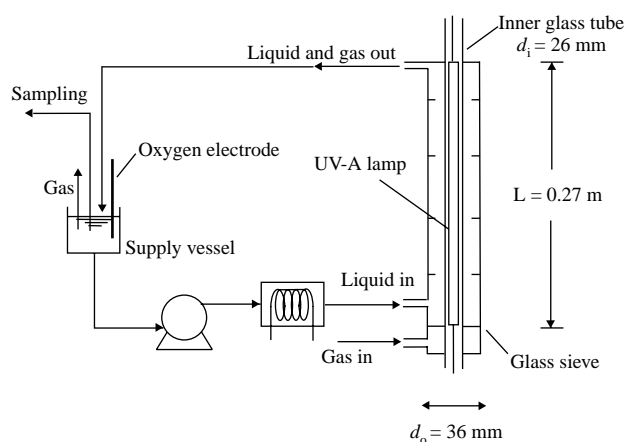


Fig. 2. Scheme of experimental set-up. Recirculating batch system consisting of supply vessel, pump, cooling device and photocatalytic reactor.

experiment, whereas at the end of the experiments the formic acid concentration will be lowest (above 95% conversion). These limiting values of the effectiveness factor will be determined to verify the assumption of the neglect of internal diffusion limitation.

### 3. Experimental methods

#### 3.1. Equipment

The experiments were performed in a  $124 \times 10^{-6} \text{ m}^3$  double wall tubular reactor of borosilicate glass, see Fig. 2. The liquid was fed tangentially into the reactor where baffles were present to reduce possible mass transfer limitations. In the inner tube a Philips TL29D15/09 (Cleo 15 W) UV-A lamp was placed. The total UV-A radiation was 1.8 W and the lamp had a wavelength spectrum of 300–410 nm with a maximum at 355 nm. The recirculating batch system consisted of a pump, cooling device, reactor and a supply vessel with a total volume of  $650 \times 10^{-6} \text{ m}^3$ . Cooling was provided by a Tamson 1000 thermostatic bath. The catalyst was coated onto the outer wall of the inner tube by dipcoating (see below). Gas (air, oxygen or nitrogen) was supplied through a glass mesh at the bottom of the reactor. A Verder gear pump V540.05 was used for liquid circulation (maximum flow rate  $25 \times 10^{-5} \text{ m}^3 \text{ s}^{-1}$ ).

The light flux of the lamp was varied by placing metal sieves (RVS, square opening 0.15 mm, thickness rod 0.15 mm; Copper, square opening 1 mm, thickness rod 0.3 mm) around the lamp in the inner tube, thereby reducing its intensity. The intensity of the light entering the reactor was determined by potassium ferrioxalate actinometry as described elsewhere (Murov, 1973) and with an UVX radiometer (sensor UVX-36, range between  $200 \mu\text{W cm}^{-2}$  and  $20 \text{ mW cm}^{-2}$ , accuracy 5%). The highest light intensity was measured with actinometry to obtain a reference value for the total light intensity entering the reactor. The

light intensities applied were measured with the UV meter and corrected with the value obtained from actinometry. The values obtained with both methods were similar.

### 3.2. Chemical substances

Degussa P-25 titanium dioxide was used as photocatalyst without further pretreatment (BET surface  $55 \text{ m}^2 \text{ g}^{-1}$ ; particles size 30 nm, forming agglomerates of 0.1–0.7  $\mu\text{m}$ ). Benzoic acid powder (Merck) was used for the determination of the mass transfer coefficients in the system. Purified water (Millipore Milli-Q) was used in the formic acid (reagent grade, Merck, 98–100%) solutions. Preliminary tests revealed that formic acid was not photodegraded by UV-A light alone. Formic acid was analyzed offline (samples taken from supply vessel) with Capillary Electrophoresis as described elsewhere (Dijkstra et al., 2001). Oxygen was analyzed on-line with an INGOLD oxygen electrode in the supply vessel.

### 3.3. Catalyst immobilization

The catalyst was adhered onto a thoroughly cleaned glass tube by dipcoating. A 5% (w/w) suspension of titanium dioxide in water was prepared in Milli-Q water and ultrasonically mixed for one hour. The glass tubes were dipped in the solution at a constant velocity of  $1.3 \text{ mm s}^{-1}$  with a dip coating apparatus as described elsewhere (Ray & Beenackers, 1998). After each dip, the layer was dried at room temperature for 10 min. The tubes with the immobilized catalyst were annealed at a temperature of 573 K for 3 h. The total amount of catalyst on the tube varied from 0 to  $3.6 \text{ g m}^{-2}$  (determined gravimetrically).

### 3.4. Experimental procedure

Prior to each experiment, the lamps were preheated for 30 min to obtain a constant light intensity. Prior to use, each coated tube was rinsed with Milli-Q water with the lamp turned on for 15 h to make sure that no pollutants were left on the catalyst surface. Experiments were performed with variable amounts of catalyst, light flux, initial formic acid and oxygen concentrations, and liquid and air flows. The temperature of the cooling water was 293 K. The Reynolds number of the liquid,  $Re_L$ , in the system was varied between 720 and 2400, corresponding to flow rates of  $3.5\text{--}12 \times 10^{-5} \text{ m}^3 \text{ s}^{-1}$ . (The residence time of the liquid in the reactor ranged from 1 to 3.5 s.) The Reynolds number of the air flow,  $Re_G$ , was varied between 1 and 62, corresponding to flows of  $0.1\text{--}5 \times 10^{-5} \text{ m}^3 \text{ s}^{-1}$ .

### 3.5. Benzoic acid dissolution method

Benzoic acid was coated on the outside of the inner tube of the reactor by dipping the tube into melted benzoic acid.

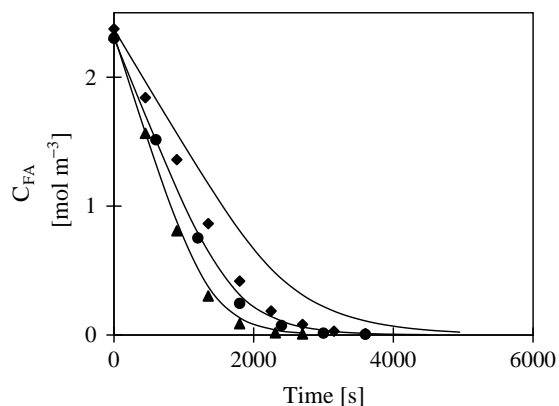


Fig. 3. Influence of  $Re_L$  on degradation rate of formic acid.  $\blacklozenge$   $Re_L = 760$   $\bullet$   $Re_L = 1433$   $\blacktriangle$   $Re_L = 2400$ ,  $w_{\text{cat}} = 3.6 \text{ g m}^{-2}$ ,  $V_{\text{liq}} = 650 \times 10^{-6} \text{ m}^3$ ,  $T = 293 \text{ K}$ ,  $I_0 = 18 \times 10^{-5} \text{ Einst m}^{-2} \text{ s}^{-1}$ ,  $Re_G = 33$ . Lines according to model (Eq. (23)) with  $k_r = 1.37$ ,  $K_1 = 0.71 \text{ m}^5 \text{ g}^{-1} \text{ mol}^{-1}$  and  $K_2 = 3.62 \text{ m}^3 \text{ mol}^{-1}$ .

The dissolution experiments were performed in the reactor by flowing water through the reactor continuously and measuring the outlet concentration of benzoic acid after a steady state was reached. The concentration of benzoic acid was determined with a UV-vis-IR spectrophotometer. Assuming that the concentration of benzoic acid at the surface is equal to the saturation concentration ( $2.6 \text{ g m}^{-3}$  (Windholz, Budavari, Stroutos, & Fertig, 1976)), the mass transfer coefficient could be determined from a steady state mass balance over the reactor.

### 3.6. Optical absorption coefficient

The optical absorption of three dipcoated layers of titanium dioxide with a known thickness was determined with a UV-vis-IR spectrophotometer as a function of the wavelength. Similar values were obtained with ellipsometric measurements (VASE Ellipsometer, Woolam). The values may give an overestimation of the absorbed radiation because scattering and reflection effects are neglected in the determination and use of the absorption coefficient.

## 4. Results

### 4.1. Mass transfer

To study the influence of external mass transport, experiments with various gas and liquid flow rates were carried out. An increase in  $Re_L$  will increase the  $k_{L,A}$  values by promoting turbulence in the system. For systems with mass transfer limitation, this will lead to higher surface concentrations of both components (Eqs. (20) and (21)) and thus to a higher reaction rate (Eq. (23)). The measurements in Fig. 3 show that indeed the degradation rate increases with increasing  $Re_L$ , indicating a certain degree of mass transport

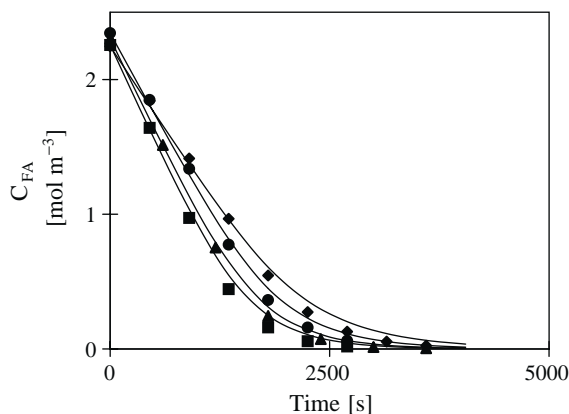


Fig. 4. Influence of  $Re_G$  on degradation rate of formic acid.  $\blacklozenge Re_G = 1$   $\bullet Re_G = 9$   $\blacktriangle Re_G = 33$   $\blacksquare Re_G = 62$ ,  $w_{cat} = 3.6 \text{ g m}^{-2}$ ,  $V_{liq} = 650 \times 10^{-6} \text{ m}^3$ ,  $T = 293 \text{ K}$ ,  $I_0 = 18 \times 10^{-5} \text{ Einst m}^{-2} \text{ s}^{-1}$ ,  $Re_L = 1433$ . Curves: model predictions.

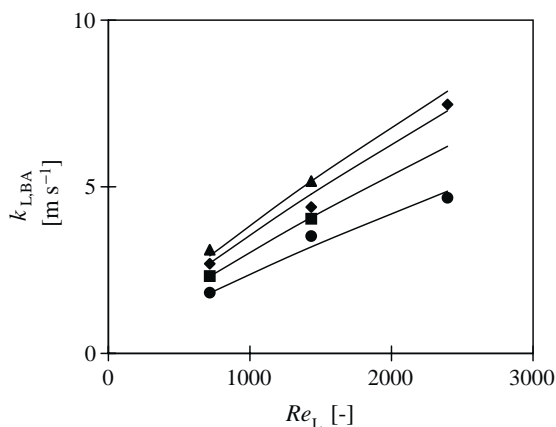


Fig. 5. Mass transfer coefficients of benzoic acid determined with dissolution method for various  $Re_L$  and  $Re_G$  numbers.  $\bullet Re_G = 1$   $\blacksquare Re_G = 9$   $\blacklozenge Re_G = 33$   $\blacktriangle Re_G = 62$ .

limitation. Fig. 4 shows that also with increasing gas flow in the reactor the degradation rate increases. Since the oxygen concentration for all these experiments remained constant at the saturation value, this increase will also be due to an increase in the mass transfer coefficient.

To quantify this effect for both formic acid and oxygen, the mass transfer coefficients,  $k_{L,A}$ , were determined with the benzoic acid (BA) dissolution method (Ray & Beenackers, 1997). In Fig. 5, the experimental values of  $k_{L,BA}$  vs.  $Re_L$  are shown at various  $Re_G$ . These could be correlated as

$$k_{L,BA} = 1.57 \times 10^{-7} Re_L^{0.73} Re_G^{0.124} \quad (30)$$

$1 < Re_G < 65$  and  $350 < Re_L < 2500$ .

Generally, mass transfer coefficients vary with the diffusivity to the power 2/3, according to  $Sh = a Re^b Sc^{1/3}$  (Perry, Green, & O'Hara Maloney, 1997). Then, with the diffusion

Table 2  
Values of kinetic parameters

Parameter	Value	95% confidence interval
$k_r$ (dimensionless)	1.37	$\pm 0.55$
$K_1$ ( $\text{m}^5 \text{g}^{-1} \text{mol}^{-1}$ )	0.71	$\pm 0.17$
$K_2$ ( $\text{m}^3 \text{mol}^{-1}$ )	3.62	$\pm 3.33$

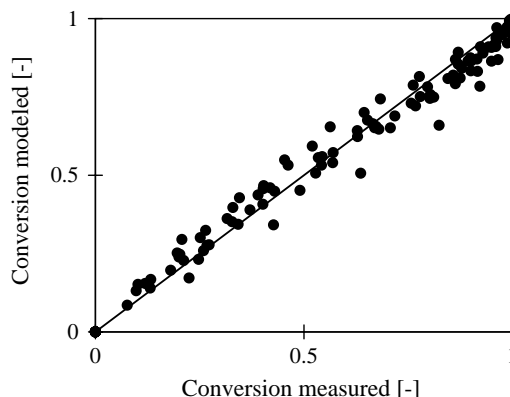


Fig. 6. Parity plot of the photocatalytic degradation of formic acid for experiments with various  $w_{cat}$  (0.42; 0.85; 1.4 and  $3.6 \text{ g m}^{-2}$ ),  $I_0$  ( $4 \times 10^{-5}$ ,  $8 \times 10^{-5}$ ,  $18 \times 10^{-5} \text{ Einst m}^{-2} \text{ s}^{-1}$ ),  $Re_L$  (760, 1433, 2400),  $Re_G$  (1, 9, 33, 62). Experiments compared to Eq. (23) with parameters taken from Table 2.

coefficients of formic acid, oxygen and benzoic acid in water,  $1.45 \times 10^{-9}$ ,  $2.5 \times 10^{-9}$  and  $0.86 \times 10^{-9} \text{ m}^2 \text{ s}^{-1}$ , respectively (Perry et al., 1997; Lide, 1995), the mass transfer coefficients of formic acid and oxygen are:

$$k_{L,FA} = 2.22 \times 10^{-7} Re_L^{0.73} Re_G^{0.124}, \quad (31)$$

$1 < Re_G < 65$  and  $350 < Re_L < 2500$ ,

$$k_{L,O_2} = 3.19 \times 10^{-7} Re_L^{0.73} Re_G^{0.124}, \quad (32)$$

$1 < Re_G < 65$  and  $350 < Re_L < 2500$ .

#### 4.2. Modeling of the kinetic constants

The parameters  $k_r$ ,  $K_1$  and  $K_2$  in Eq. (16) have been determined by fitting the model (Eqs. (2), (3), (20), (21), (23), (31), (32)) to the experimental data obtained with variable  $Re_G$  (1–33),  $w_{cat}$  ( $0.42$ – $3.6 \text{ g m}^{-2}$ ) and  $I_0$  ( $4 \times 10^{-5}$  –  $18 \times 10^{-5} \text{ Einst m}^{-2} \text{ s}^{-1}$ ) for  $Re_L$  (1433) and  $C_{0,FA}$  ( $2.2 \text{ mol m}^{-3}$ ) using the Levenberg–Marquadt method (Press, Flannery, Teukolsky, & Vetterling, 1989). The results are shown in Table 2 together with the 95% confidence interval determined with the Student's distribution (Kreyszig, 1999). Good agreement of the modeled and measured transient conversions is obtained, as shown in the parity plot of Fig. 6.

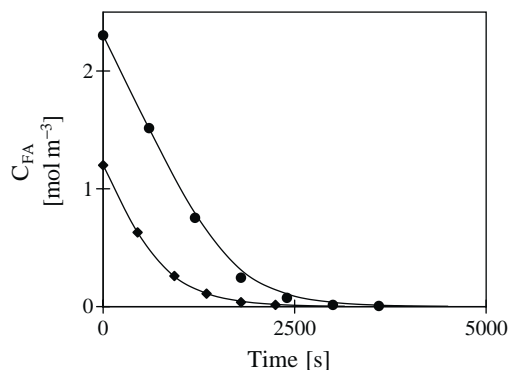


Fig. 7. Influence of initial concentration of formic acid on the degradation rate.  $\blacklozenge C_{FA,0} = 1.2 \text{ mol m}^{-3}$   $\bullet C_{FA,0} = 2.3 \text{ mol m}^{-3}$ .  $w_{\text{cat}} = 3.6 \text{ g m}^{-2}$ ,  $I_0 = 18 \times 10^{-5} \text{ Einst m}^{-2} \text{ s}^{-1}$ ,  $Re_G = 33$ ,  $Re_L = 1433$ ,  $V_{\text{liq}} = 650 \times 10^{-6} \text{ m}^3$ ,  $T = 293 \text{ K}$ . Curves: model predictions.

#### 4.3. Internal diffusion limitation

The values of the effectiveness factors for both limiting situations (i.e.  $\eta_{FA}$  and  $\eta_{O_2}$ ) show that diffusion limitation is only significant with the thickest catalyst layer and the highest light intensity ( $w_{\text{cat}} = 3.6 \text{ g m}^{-2}$  and  $I_0 = 18 \times 10^{-5} \text{ Einst m}^{-2} \text{ s}^{-1}$ ), see Table 3. Experiments under these circumstances were not taken into account in the determination of the parameters shown in Table 2. When modeling the latter experiments, the data are still well described with the obtained parameters and without taking the effectiveness factor into account (see Fig. 7), due to the high degree of external mass transfer limitation controlling the conversion rate in these experiments ( $C_s/C_b \approx 0.2$ , see below).

#### 4.4. Influence of experimental parameters

As explained above,  $Re_G$  and  $Re_L$  influence the degradation by changing the value of the mass transfer coefficients and hereby changing the surface concentrations which determine the reaction rate. The lines in Fig. 4 were calculated with the model including the influence of  $Re_G$  and  $Re_L$  on the  $k_{L,A}$  values (Eqs. (31) and (32)), and show a good agreement with the experimental data. This indicates that the dependence of the mass transfer coefficients on the Reynolds number of the gas flow can reasonably well be described with relations (31) and (32). Calculations with variable  $Re_L$  show a deviation between the model and the experiments for the lowest Reynolds number (see Fig. 3), probably due to inaccuracies in the measurements of  $k_L$ .

Formic acid is degraded directly to  $\text{CO}_2$  and water. Therefore, the developed kinetic model should be independent of intermediates or inhibiting by-products. To confirm this independence, two experiments with different initial concentration were carried out. Fig. 7 shows that the model describes the measurements accurately.

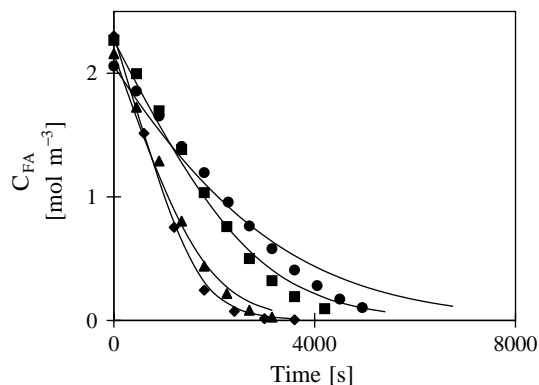


Fig. 8. Influence of layer thickness on degradation rate of formic acid.  $\bullet w_{\text{cat}} = 0.42 \text{ g m}^{-2}$   $\blacksquare w_{\text{cat}} = 0.85 \text{ g m}^{-2}$   $\blacktriangle w_{\text{cat}} = 1.4 \text{ g m}^{-2}$   $\blacklozenge w_{\text{cat}} = 3.6 \text{ g m}^{-2}$ ,  $I_0 = 18 \times 10^{-5} \text{ Einst m}^{-2} \text{ s}^{-1}$ ,  $Re_G = 33$  ( $Re_G = 1$  for  $w_{\text{cat}} = 0.85 \text{ g m}^{-2}$ ),  $Re_L = 1433$ ,  $V_{\text{liq}} = 650 \times 10^{-6} \text{ m}^3$ ,  $T = 293 \text{ K}$ . Curves: model predictions.

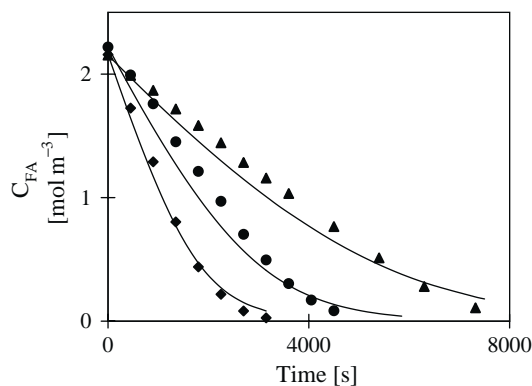


Fig. 9. Influence of light flux on degradation rate.  $\blacktriangle I_0 = 4 \times 10^{-5} \text{ Einst m}^{-2} \text{ s}^{-1}$   $\bullet I_0 = 8 \times 10^{-5} \text{ Einst m}^{-2} \text{ s}^{-1}$   $\blacklozenge I_0 = 18 \times 10^{-5} \text{ Einst m}^{-2} \text{ s}^{-1}$ ,  $w_{\text{cat}} = 1.4 \text{ g m}^{-2}$ ,  $Re_G = 33$ ,  $Re_L = 1433$ ,  $V_{\text{liq}} = 650 \times 10^{-6} \text{ m}^3$ ,  $T = 293 \text{ K}$ . Curves: model predictions.

Eq. (2) shows that by increasing the layer thickness the absorbed light intensity and thus the amount of holes and electrons generated will increase to a maximum. The layer thickness which absorbs 90% of the light is  $0.8 \mu\text{m}$  (Lambert–Beer (Braun, Maurette, & Oliveros, 1991)) for  $\lambda = 355 \text{ nm}$  corresponding to an amount of catalyst of  $1.3 \text{ g m}^{-2}$ . Increasing the amount of catalyst above this value will hardly raise the number of charge carriers any further, though some extra activity above  $0.8 \mu\text{m}$  may still result from the adsorption term for formic acid,  $\theta_{FA}$ , which is also a function of the layer thickness:

$$\theta_{FA} = \frac{w_{\text{cat}} K_1 C_{s,FA}}{1 + w_{\text{cat}} K_1 C_{s,FA}} \quad (33)$$

The dependency of the degradation rate on the amount of catalyst appears to be described rather nicely with the model developed (see Fig. 8), as is the influence of variations of the light flux (see Fig. 9).

Table 3  
Influence of internal and external mass transfer limitation

$w_{\text{cat}}$ $\text{g m}^{-2}$	$I_0$ $\text{Einst m}^{-2} \text{s}^{-1}$	$C_{b,FA}$ $\text{mol m}^{-3}$	$C_{s,FA}/C_{b,FA}$	$C_{s,O_2}/C_{b,O_2}$	$\eta_{FA}$	$\eta_{O_2}$
0.42	$8 \times 10^{-5}$	2.15 0.1	0.93 0.89	0.82 0.99	1	1
0.42	$18 \times 10^{-5}$	2.06 0.1	0.86 0.77	0.65 0.97	1	0.99
0.85	$18 \times 10^{-5}$	2.27 0.1	0.76 0.44	0.32 0.93	0.98	0.95
1.4	$4 \times 10^{-5}$	2.15 0.1	0.91 0.77	0.77 0.97	0.99	0.98
1.4	$8 \times 10^{-5}$	2.22 0.1	0.85 0.60	0.57 0.95	0.97	0.96
1.4	$18 \times 10^{-5}$	2.16 0.1	0.75 0.40	0.34 0.90	0.94	0.90
3.6	$4 \times 10^{-5}$	2.31 0.1	0.89 0.57	0.70 0.96	0.93	0.94
3.6	$8 \times 10^{-5}$	2.42 0.1	0.82 0.36	0.47 0.92	0.85	0.86
3.6	$18 \times 10^{-5}$	2.3 0.1	0.74 0.19	0.25 0.89	0.72	0.70

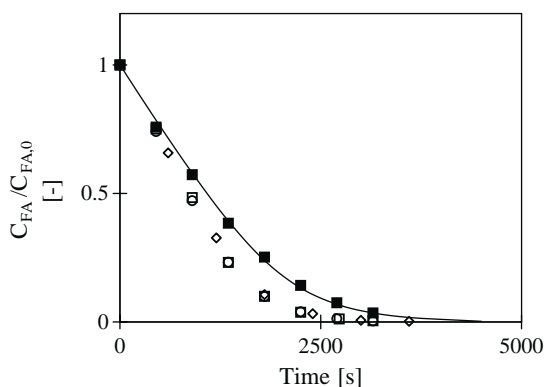


Fig. 10. Standard experiments to establish activity of catalyst with time.  $\diamond$  First experiment,  $\square$  fifth experiment,  $\circ$  12th experiment,  $\blacksquare$  deactivated experiment with modeling (line).  $w_{\text{cat}} = 3.6 \text{ g m}^{-2}$ ,  $I_0 = 18 \times 10^{-5} \text{ Einst m}^{-2} \text{s}^{-1}$ ,  $Re_G = 33$ ,  $Re_L = 1433$ ,  $V_{\text{liq}} = 650 \times 10^{-6} \text{ m}^3$ ,  $T = 293 \text{ K}$ .

The activity of the catalyst during the various experiments remained constant, see Fig. 10. However, when the catalyst tube was removed from the reactor and placed in open air for a month, considerable deactivation was observed, as is also shown in Fig. 10. The value of the kinetic parameter  $k_r$  for this deactivated experiment was determined to be 0.71 instead of the previous 1.37 while keeping  $K_1$  and  $K_2$  at the same values. The deactivation is probably caused by adsorption of pollutants from the air.

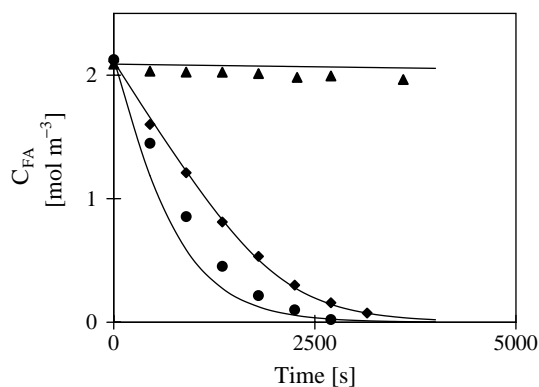


Fig. 11. Influence of oxygen concentration on formic acid degradation rate. Gas added to the system:  $\blacktriangle$  nitrogen  $\blacklozenge$  air  $\bullet$  oxygen.  $w_{\text{cat}} = 3.6 \text{ g m}^{-2}$ ,  $I_0 = 18 \times 10^{-5} \text{ Einst m}^{-2} \text{s}^{-1}$ ,  $Re_G = 33$ ,  $Re_L = 1433$ ,  $V_{\text{liq}} = 650 \times 10^{-6} \text{ m}^3$ ,  $T = 293 \text{ K}$ . Lines according to model (Eq. (23)) with  $k_r = 0.71$ ,  $K_1 = 0.71 \text{ m}^5 \text{ g}^{-1} \text{ mol}^{-1}$  and  $K_2 = 3.62 \text{ m}^3 \text{ mol}^{-1}$ .

The oxygen concentration was varied from  $0.28$  to  $1.4 \text{ mol m}^{-3}$  and to  $0 \text{ mol m}^{-3}$  by using air, pure oxygen and nitrogen, respectively. With pure oxygen the degradation rate of formic acid increased significantly, see Fig. 11. As expected, the photocatalytic degradation was negligible with nitrogen since no electron acceptor was present in the system. The model appears to describe the dependency of the degradation rate on the oxygen concentration rather well ( $k_r = 0.71$ ), see Fig. 11.

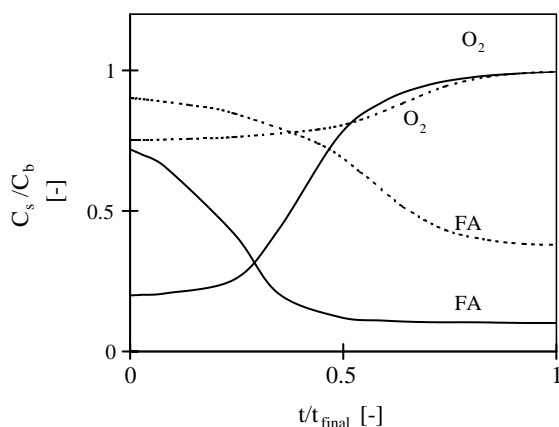


Fig. 12.  $C_s/C_b$  ratio vs. normalized time for oxygen and formic acid during a typical degradation experiment. Dashed lines:  $w_{\text{cat}} = 0.42 \text{ g m}^{-2}$ , solid lines:  $w_{\text{cat}} = 3.6 \text{ g m}^{-2}$ .  $I_0 = 18 \times 10^{-5} \text{ Einst m}^{-2} \text{ s}^{-1}$ ,  $Re_G = 33$ ,  $Re_L = 1433$ ,  $V_{\text{liq}} = 650 \times 10^{-6} \text{ m}^3$ ,  $T = 293 \text{ K}$ .

## 5. Discussion

### 5.1. External mass transfer

The extent of external mass transfer limitation for a component can be estimated from the ratio of the surface and the bulk concentration ( $C_s/C_b$ ), which varies between 0 and 1 for total and no mass transfer limitation, respectively.

For experiments with the highest and lowest amounts of catalyst this ratio is shown for both formic acid and oxygen against the normalized reaction time ( $t/t_{\text{final}}$ ) in Fig. 12. Initially, the bulk concentration of formic acid is much higher than that of oxygen (2.2 vs. 0.28 mol  $\text{m}^{-3}$ , resp.) resulting in mass transfer limitation of oxygen, which is confirmed by the low ratio of  $C_{s,O_2}/C_{b,O_2}$ . At the end of the experiment formic acid is mass transfer limited as is indicated by the lower value of  $C_{s,FA}/C_{b,FA}$ , with no oxygen limitation anymore.

For lower amounts of catalyst the activity of the catalyst per unit reactor volume will be less, whereas the mass transfer rate is only a function of the hydrodynamics in the system and will thus remain constant. Therefore, for lower amounts of catalyst, the degree of mass transfer limitation will be less than for higher amounts of catalyst. Fig. 12 shows that indeed the  $C_s/C_b$  ratio for both components is higher for the lowest amount of catalyst.

### 5.2. Accuracy of model

Instead of by the reaction between adsorbed formic acid and hydroxyl radicals, the model can also be represented by the direct reaction between adsorbed formic acid and holes. If the reaction between hydroxyl radicals and formic acid is neglected, this model can be simplified to the same form as Eq. (16) and will thus be able to describe the measurements. Therefore, whether the reaction proceeds via

the hydroxyl radical or via direct uptake of a hole in the semiconductor cannot be distinguished from the measurements. Also Turchi and Ollis (1990) found that the actual reaction mechanism could not be distinguished from the measurements.

In literature, the reaction between oxygen and an electron is also mentioned as determining the reaction rate (Gerischer & Heller, 1991; Cornish, Lawton, & Robertson, 2000). For this reaction, the resulting rate equation is

$$R_{FA} = \frac{kKeg[\text{O}_{2,\text{ads}}]a_{\text{ext}}}{(1 + K[\text{O}_{2,\text{ads}}])} \quad (34)$$

This equation apparently cannot describe the measurements. Since the concentration of oxygen was kept constant during the experiments, a time independent rate is predicted by Eq. (34) which is conflicting with the observed decrease of rate with time (and with decreasing acid concentration).

The adsorption of both oxygen and formic acid seem to be a crucial step in the degradation. If the adsorption of formic acid is not taken into account, Eq. (16) reduces to

$$R_{FA} = \frac{kegK_{\text{ads1}}[FA]K_{\text{ads2}}[\text{O}_2]a_{\text{ext}}}{(1 + K_{\text{ads1}}[FA])(1 + K_{\text{ads2}}[\text{O}_2])} \quad (35)$$

which cannot describe the measurements either, as the residual sum of squares obtained by applying Eq. (35) appeared to be 4 times higher than that obtained with the model presented.

Although the adsorption of formic acid and oxygen at the catalyst seems to play an important role in the degradation, the mechanism by which this adsorption in the dark part of the titanium layer can be beneficial to the degradation is not fully clear. Probably, the electrons diffuse over the semiconductor layer, as suggested by Kelly and Vanmaekelbergh (1998). Formic acid reacts with a hole or a hydroxyl radical. The adsorption of formic acid at the dark side of the catalyst has a positive effect on the degradation rate, maybe due to diffusion of radicals over the layer and holes in the layer.

The model is limited to a restricted region of light intensities ( $4 \times 10^{-5} < I_0 < 18 \times 10^{-5} \text{ Einst m}^{-2} \text{ s}^{-1}$ ). For high light intensities, the linear dependency between the degradation rate and the light intensity may get lost (Egerton & King, 1979; Hoffmann et al., 1995).

### 5.3. Quantum yield

The apparent quantum yield,  $\Phi$ , is used as a direct measure for the efficiencies of the heterogeneous photocatalytic processes. For a batch system, it is defined as (Hoffmann et al., 1995):

$$\Phi = \frac{(dC/dt)V_{\text{liq}}}{I} \quad (36)$$

Table 4  
Theoretical and measured apparent quantum yields

$I_0$ (Einst $\text{m}^{-2} \text{s}^{-1}$ )	$\Phi$ measured <sup>a</sup>	$\Phi$ calculated (no mass transfer limitation)
$4 \times 10^{-5}$	0.45	0.5
$8 \times 10^{-5}$	0.4	0.5
$18 \times 10^{-5}$	0.23	0.5

<sup>a</sup>Experimental data:  $w_{\text{cat}} = 3.6 \text{ g m}^{-2}$ ,  $Re_L = 1433$ ,  $Re_G = 33$ ,  $C_{b,FA} = 2.2 \text{ mol m}^{-3}$ ,  $C_{b,O_2} = 0.3 \text{ mol m}^{-3}$ .

with  $dC/dt$  the initial degradation rate of the model component ( $\text{mol m}_{\text{liq}}^{-3} \text{s}^{-1}$ ). For the values of the light fluxes applied (0 to  $1.8 \times 10^{-4}$  Einst  $\text{m}^{-2} \text{s}^{-1}$ ) the degradation rate linearly depends on the light flux (Eqs. (2) and (16)), resulting in a constant apparent quantum yield in case of negligible mass transfer limitation, see Table 4. In reality, the apparent quantum yield increases with decreasing light flux because of a decreasing degree of mass transfer limitation. Theoretically, the apparent quantum yield can be increased up to 0.5 by eliminating any mass transfer limitation.

The apparent quantum yields observed are high (up to 0.45) compared to literature values for other components, which lay in the range of 0.06–0.001 (Mills et al., 1993; Legrini, Oliveros, & Braun, 1993). Similar high values were obtained for formic acid by Buechler, Nam, Zawistowski, Noble, and Koval (1999). A reason for the high apparent quantum yield in formic acid degradation may be found in the second degradation step given by reaction R10 in Table 1. Only one hole is necessary for the total degradation of formic acid and reaction R10 can even increase the radical production.

## 6. Conclusions

A simple kinetic model describes the degradation of formic acid in an immobilized photocatalytic reactor as a function of the formic acid and the oxygen concentration, the layer thickness and the light flux. The degradation is represented by the reaction of adsorbed hydroxyl radicals or holes with adsorbed formic acid. Measurements in a three phase (*G-L-S*) tubular reactor showed that mass transfer limitation occurred in the system. The mass transfer coefficient was measured with the benzoic acid method as a function of the Reynolds number of both the liquid and the gas phase. Kinetic parameters independent on the reactor configuration could be determined from the degradation experiments taking into account any effects of mass transfer limitation. The adsorption of oxygen and formic acid at the catalyst layer appears to play an important role in this photocatalytic system. For the range of light fluxes applied, a linear dependency of the degradation rate on the light flux was found. Rather high apparent quantum efficiencies up to 0.45 were observed.

## Notation

$a_s$	specific internal surface area, $\text{m}_{\text{cat}}^2 \text{m}_{\text{reac}}^{-3}$
$a_{\text{ext}}$	specific external surface area, $\text{m}_{\text{ext cat}}^2 \text{m}_{\text{reac}}^{-3}$
$A_{\text{ext}}$	external catalyst area, $\text{m}^2$
$C$	concentration, $\text{mol m}^{-3}$
$C_s$	surface concentration, $\text{mol m}^{-3}$
$C_b$	bulk concentration, $\text{mol m}^{-3}$
$d_h$	hydraulic diameter ( $=d_i-d_o$ ), m
$d_i$	diameter inner tube, m
$d_o$	diameter outer tube, m
$d_L$	layer thickness ( $=V_{\text{cat}}/A_{\text{ext}}$ ), m
$D$	diffusivity, $\text{m}^2 \text{s}^{-1}$
$D_{\text{eff}}$	effective diffusivity, $\text{m}^2 \text{s}^{-1}$
$e$	equivalence constant, $\text{mol Einst}^{-1}$
$[FA]$	concentration of formic acid, $\text{mol m}^{-3}$
$[FA_{\text{ads}}]$	concentration of adsorbed formic acid, $\text{mol m}_{\text{reac}}^{-3}$
$g$	generation rate of charge carriers, Einst $\text{m}^{-2} \text{s}^{-1}$
$g(x, \lambda)$	generation rate of charge carriers per wavelength, at position $x$ in the layer, Einst $\text{m}^{-3} \text{s}^{-1} \text{nm}^{-1}$
$g(\lambda)$	generation rate of charge carriers per wavelength, Einst $\text{m}^{-2} \text{s}^{-1} \text{nm}^{-1}$
$I$	total amount of photons entering reactor, Einst $\text{s}^{-1}$
$I_0$	light flux entering reactor, Einst $\text{m}^{-2} \text{s}^{-1}$
$I_0(\lambda)$	light flux entering reactor per wavelength, Einst $\text{m}^{-2} \text{s}^{-1} \text{nm}^{-1}$
$k_L$	mass transfer coefficient, $\text{m s}^{-1}$
$k_r$	kinetic constant, dimensionless
$k_s, k_T$	proportionality constant (Eq. (14) resp. (15)), $\text{mol g}^{-1} \text{m}^{-1}$
$k_{2+}, k_{5+}, k_{7a}, k_{7b}, k_8$	rate constants, $\text{m}^4 \text{mol}^{-1} \text{s}^{-1}$
$k_{5+}^1, k_{5-}$	rate constants, $\text{m s}^{-1}$
$K_1$	adsorption constant, $\text{m}^5 \text{g}^{-1} \text{mol}^{-1}$
$K_2, K_{19}, K_{20}$	adsorption constant, $\text{m}^3 \text{mol}^{-1}$
$n$	concentration of electrons, $\text{mol m}_{\text{reac}}^{-3}$
$[\cdot \text{OH}_{\text{ads}}]$	concentration of adsorbed hydroxyl radicals, $\text{mol m}_{\text{reac}}^{-3}$
$[\text{O}_2]$	concentration of oxygen in solution, $\text{mol m}^{-3}$
$[\text{O}_{2\text{ads}}]$	concentration of adsorbed oxygen, $\text{mol m}_{\text{reac}}^{-3}$
$p$	concentration of holes, $\text{mol m}_{\text{reac}}^{-3}$
$R_{FA}$	reaction rate per unit reactor volume, $\text{mol m}_{\text{reac}}^{-3} \text{s}^{-1}$
$R_{FA, \text{cat}}$	reaction rate per unit catalyst volume, $\text{mol m}_{\text{cat}}^{-3} \text{s}^{-1}$
$Re_G$	Reynolds number gas ( $=\rho_G v_G d_h / \eta_G$ ), dimensionless
$Re_L$	Reynolds number liquid ( $=\rho_L v_L d_h / \eta_L$ )

$Sc$	Schmidt number(= $\eta_L/D\rho_L$ ), dimensionless
[site]	concentration of vacant sites, $\text{mol m}_{\text{react}}^{-3}$
[site] <sub>tot</sub>	total concentration of sites, $\text{mol m}_{\text{react}}^{-3}$
$Sh$	Sherwood number(= $k_L d_h/D$ ), dimensionless
$t$	time, s
$t_{\text{final}}$	experimental time with $C_{b,FA}$ of $5 \times 10^{-3} \text{ mol m}^{-3}$ , s
[ $T$ ]	concentration of traps in layer, $\text{mol m}_{\text{react}}^{-3}$
$T$	temperature, K
$v$	superficial velocity, empty column, $\text{m s}^{-1}$
$V_{\text{cat}}$	catalyst volume, $\text{m}^3$
$V_{\text{liq}}$	total liquid volume, $\text{m}^3$
$V_{\text{react}}$	reactor volume (annular space), $\text{m}^3$
$w_{\text{cat}}$	catalyst loading, $\text{g m}^{-2}$
$x$	distance into the semiconductor layer, m

### Greek letters

$\alpha$	optical absorption coefficient, $\text{m}^{-1}$
$\epsilon_{\text{cat}}$	porosity of catalyst layer, dimensionless
$\eta$	effectiveness factor, dimensionless
$\eta$	viscosity fluid, Pa s
$\theta_{FA}$	adsorption term of formic acid, dimensionless
$\kappa$	proportionality constant, dimensionless
$\lambda$	wavelength of light, nm
$\rho$	density fluid, $\text{kg m}^{-3}$
$\tau$	tortuosity, dimensionless
$\phi$	Thiele modulus, see Eq. (28), dimensionless
$\Phi$	apparent quantum yield, dimensionless

### sub- and superscripts

$A$	component $A$
$BA$	benzoic acid
$FA$	formic acid
$O_2$	oxygen

### Acknowledgements

This work was supported by the Netherlands Foundation for Chemical Research (SON) and the Netherlands Technology Foundation. We acknowledge the generous supply of UV lamps by Philips, Eindhoven, and Horst Buwalda for the experimental work performed in this project.

### References

- Bideau, M., Claudel, B., & Otterbein, M. (1980). Photocatalysis of formic acid oxidation by oxygen in an aqueous medium. *Journal Photochemistry*, *14*, 291–302.
- Blake, D. M., Webb, J., Turchi, C., & Magrini, K. (1991). Kinetic and mechanistic overview of  $\text{TiO}_2$ -photocatalyzed oxidation reactions in aqueous solution. *Solar Energy Materials*, *24*, 584–593.
- Braun, A. M., Maurette, M. -T., & Oliveros, E. (1991). *Photochemical technology*. Chichester: Wiley.
- Buechler, K. J., Nam, C. H., Zawistowski, T. M., Noble, R. D., & Koval, C. A. (1999). Design and evaluation of a novel-controlled periodic illumination reactor to study photocatalysis. *Industrial and Engineering Chemistry Research*, *38*, 1258–1263.
- Butler, M. A. (1977). Photoelectrolysis and physical properties of the semiconducting electrode  $\text{WO}_3$ . *Journal of Applied Physics*, *48*(5), 1914–1920.
- Carraway, E. R., Hoffman, A. J., & Hoffmann, M. R. (1994). Photocatalytic oxidation of organic acids on quantum-sized semiconductor colloids. *Environmental Science and Technology*, *28*, 786–793.
- Chen, J., Ollis, D. F., Rulkens, W. H., & Bruning, H. (1999). Photocatalyzed oxidation of alcohols and organochlorides in the presence of native  $\text{TiO}_2$  and metallized  $\text{TiO}_2$  suspensions. Part (II): Photocatalytic mechanisms *Water Research*, *33*(3), 669–676.
- Chen, H. Y., Zahraa, O., Bouchy, M., Thomas, F., & Bottero, J. Y. (1995). Adsorption properties of  $\text{TiO}_2$  related to the photocatalytic degradation of organic contaminants in water. *Journal of Photochemistry and Photobiology*, *85*, 179–186.
- Cornish, B. J. P. A., Lawton, L. A., & Robertson, P. K. J. (2000). Hydrogen peroxide enhanced photocatalytic oxidation of microcystin-LR using titanium dioxide. *Applied Catalysis B*, *25*(1), 59–67.
- Dijkstra, M. F. J., Buwalda, H., Jong, A. W. F. de., Michorius, A., Winkelman, J. G. M., & Beenackers, A. A. C. M. (2001). Experimental comparison of three reactor designs for photocatalytic water purification. *Chemical Engineering Science*, *56*(2), 547–555.
- Dillert, R., & Bahnemann, D., (1996). Photocatalytic Water treatment: Chances and limitations, In: A. Vogelpohl (Ed.), *International conference oxidation technology for water and wastewater treatment*. CUTEC Schriftenreihe nr. 23, Clausthal-Zellerfeld: Papierflieger Verlag.
- Egerton, T. A., & King, C. J. (1979). The influence of light intensity on photoactivity in  $\text{TiO}_2$  pigmented systems. *J. Oil Col. Chem. Assoc.*, *62*, 386–391.
- Emeline, A. V., Ryabchuk, V., & Serpone, N. (2000). Factors affecting the efficiency of a photocatalyzed process in aqueous metal-oxide dispersions: Prospects of distinguishing between two kinetic models *Journal of Photochemistry and Photobiology A*, *133*, 89–97.
- Fox, M. A., & Dulay, M. T. (1993). Heterogeneous photocatalysis. *Chemical Reviews*, *93*, 341–357.
- Froment, G. F., & Bischoff, K. B. (1979). *Chemical reactor analysis and design*. New York: Wiley.
- Gerischer, H. (1995). Photocatalysis in aqueous solution with small  $\text{TiO}_2$  particles and the dependence of the quantum yield on particle size and light intensity. *Electrochimica Acta*, *40*(10), 1277–1281.
- Gerischer, H., & Heller, A. (1991). The role of oxygen in photooxidation of organic molecules on semiconductor particles. *Journal of Physical Chemistry*, *95*(13), 5261–5267.
- Halmann, M. M. (1996). *Photodegradation of water pollutants*. Boca Raton: CRC Press.
- Hoffmann, M. R., Martin, S. T., Choi, W., & Bahnemann, D. W. (1995). Environmental applications of semiconductor photocatalysis. *Chemical Reviews*, *95*, 69–96.
- Howe, R. F., & Grätzel, M. (1985). EPR observation of trapped electrons in colloidal  $\text{TiO}_2$ . *Journal of Physical Chemistry*, *89*, 4495–4499.
- Jacobs, J. W. M. (1998). *Laser-initiated metal deposition on semiconductors from aqueous solutions*. Thesis, University of Utrecht.
- Jongh, P. E. de., & Vanmaekelbergh, D. (1996). Trap-limited electronic transport in assemblies of nanometer-size  $\text{TiO}_2$  particles. *Physics Review Letters*, *77*(6), 3427–3430.
- Kelly, J. J., & Vanmaekelbergh, D. (1998). Charge carrier dynamics in nanoporous photoelectrodes. *Electrochimica Acta*, *43*(19–20), 2773–2780.
- Kesselman, J. M., Weres, O., Lewis, N. S., & Hoffmann, M. R. (1997). Electrochemical production of hydroxyl radical at polycrystalline Nb-doped  $\text{TiO}_2$  electrodes and estimation of the partitioning between hydroxyl radical and direct hole oxidation pathways. *Journal of Physical Chemistry B*, *101*, 2637–2643.

- Kreyszig, E. (1999). *Advanced engineering mathematics* (8th ed.). Singapore: Wiley.
- Lawless, D., Serpone, N., & Meisel, D. (1991). Role of OH radicals and trapped holes in photocatalysis. A pulse radiolysis study. *Journal of Physical Chemistry*, *95*, 5166–5170.
- Legrini, O., Oliveros, E., & Braun, A. M. (1993). Photochemical processes for water treatment. *Chemical Reviews*, *93*, 671–698.
- Lide, D. R. (1995). *CRC Handbook of chemistry and physics* (75th ed.). Boca Raton: CRC Press.
- Martin, S. T., Herrmann, H., Choi, W., & Hoffmann, M. R. (1994). Time-resolved microwave conductivity. Part 1—TiO<sub>2</sub> photoreactivity and size quantization. *Journal of Chemical Society of Faraday Transactions*, *90*(21), 3315–3322.
- Matthews, R. W., & McEvoy, S. R. (1992). Photocatalytic degradation of phenol in the presence of near-UV illuminated titanium dioxide. *Journal of Photochemistry and Photobiology A*, *64*, 231–246.
- Mills, A., Davies, R. H., & Worsley, D. (1993). Water purification by semiconductor photocatalysis. *Chemical Society Reviews*, 417–425.
- Mills, A., & Le Hunte, S. (1997). An overview of semiconductor photocatalysis. *Journal of Photochemistry and Photobiology A*, *108*, 1–35.
- Minero, C., Aliberti, C., Pelizzetti, E., Terzian, R., & Serpone, N. (1991). Kinetic studies in heterogeneous photocatalysis. 6. AM1 simulated sunlight photodegradation over titania in aqueous media: A first case of fluorinated aromatics and identification of intermediates *Langmuir*, *7*, 928–936.
- Murov, S. L. (1973). *Handbook of photochemistry* (pp. 119–123). New York: Dekker.
- Okamoto, K., Yamamoto, Y., Tanaka, H., Tanaka, M., & Itaya, A. (1985). Heterogeneous photocatalytic decomposition of phenol over TiO<sub>2</sub> powder. *Bulletin of Chemical Society of Japan*, *58*, 2015–2022.
- Ollis, D. F., Pelizzetti, E., & Serpone, N. (1991). Photocatalyzed destruction of water contaminants. *Environmental Science and Technology*, *25*(9), 1522–1529.
- Pelizzetti, E., & Minero, C. (1993). Mechanism of the photo-oxidative degradation of organic pollutants over TiO<sub>2</sub> Particles. *Electrochimica Acta*, *38*(1), 47–55.
- Perry, R. H., Green, D. W., & O'Hara Maloney, J. (1997). *Perry's chemical engineers' handbook* (7th ed.). New York: McGraw-Hill.
- Peterson, M. W., Turner, J. A., & Nozik, A. J. (1991). Mechanistic studies of the photocatalytic behavior of TiO<sub>2</sub>. Particles in a photoelectrochemical slurry cell and the relevance to photodetoxification reactions. *Journal of Physical Chemistry*, *95*, 221–225.
- Prairie, M. R., Evans, L. R., Stange, B. M., & Martinez, S. L. (1993). An Investigation of TiO<sub>2</sub> photocatalysis for the treatment of water contaminated with metals and organic chemicals. *Environmental Science and Technology*, *27*(9), 1776–1782.
- Press, W. H., Flannery, B. P., Teukolsky, S. A., & Vetterling, W. T. (1989). *Numerical recipes in Pascal: The art of scientific computing*. Cambridge: Cambridge University Press.
- Ray, A. K., & Beenackers, A. A. C. M. (1997). Novel swirl-flow reactor for kinetic studies of semiconductor photocatalysis. *AIChE Journal*, *43*(10), 2571–2578.
- Ray, A. K., & Beenackers, A. A. C. M. (1998). Novel photocatalytic reactor for water purification. *AIChE Journal*, *44*(2), 477–483.
- Tan, M. X., Laibinis, P. E., Nguyen, S. T., Kesselman, J. M., Stanton, C. E., & Lewis, N. S. (1994). Principles and applications of semiconductor photoelectrochemistry. In K. D. Karlin (Ed.), *Progress in inorganic chemistry*, Vol. 41. New York: Wiley.
- Turchi, C. S., & Ollis, D. F. (1990). Photocatalytic degradation of organic water contaminants: Mechanisms involving hydroxyl radical attack *Journal of Catalysis*, *122*, 178–192.
- Upadhy, S., & Ollis, D. F. (1997). Simple photocatalysis model for photoefficiency enhancement via controlled, periodic illumination. *Journal of Physical Chemistry B*, *101*, 2625–2631.
- Westerterp, K. R., Swaaij, W. P. M. van., & Beenackers, A. A. C. M. (1984). *Chemical reactor design and operation* (2nd ed.). Chichester: Wiley.
- Windholz, M., Budavari, S., Strountsos, L. Y., & Fertig, M. N. (1976). *The Merck index: An encyclopedia of chemicals and drugs* (9th ed.). Rayway USA: Merck & Co.
- Yue, P. L. (1992). Degradation of organic pollutants by advanced oxidation. *Transactions I.Chem.E.*, *70*(Part B), 145–148.